

MICROBIAL FUEL CELLS

Silver nanoparticles boost charge-extraction efficiency in *Shewanella* microbial fuel cells

Bocheng Cao^{1,2}, Zipeng Zhao², Lele Peng¹, Hui-Ying Shiu², Mengning Ding², Frank Song¹, Xun Guan¹, Calvin K. Lee³, Jin Huang², Dan Zhu¹, Xiaoyang Fu¹, Gerard C. L. Wong³, Chong Liu¹, Kenneth Nealon⁵, Paul S. Weiss^{1,2,3,4}, Xiangfeng Duan^{1,4*}, Yu Huang^{2,4*}

Microbial fuel cells (MFCs) can directly convert the chemical energy stored in organic matter to electricity and are of considerable interest for power generation and wastewater treatment. However, the current MFCs typically exhibit unsatisfactorily low power densities that are largely limited by the sluggish transmembrane and extracellular electron-transfer processes. Here, we report a rational strategy to boost the charge-extraction efficiency in *Shewanella* MFCs substantially by introducing transmembrane and outer-membrane silver nanoparticles. The resulting *Shewanella*-silver MFCs deliver a maximum current density of 3.85 milliamperes per square centimeter, power density of 0.66 milliwatts per square centimeter, and single-cell turnover frequency of 8.6×10^5 per second, which are all considerably higher than those of the best MFCs reported to date. Additionally, the hybrid MFCs feature an excellent fuel-utilization efficiency, with a coulombic efficiency of 81%.

Microbial fuel cells (MFCs) can directly convert chemical energy stored in many sources of biodegradable organic matter to electrical energy through microorganism metabolism (1, 2). A diverse range of bacterial species (3) and the wide range of fuels (4, 5) make MFCs an attractive technology for renewable bioelectricity power generation from biomass and wastewater treatment (6). For this reason, MFCs have attracted increasing attention from academic and industrial communities (7).

Among the bacteria that power these systems, *Shewanella* species are widely studied for bioremediation and environmental energy recovery because of their robust growth in both aerobic and anaerobic environments (8) and rich distribution in soil and seawater (9). However, the current density and power density obtained from typical *Shewanella* MFCs are generally too low for practical applications (4, 10). The low power output is largely limited by the bacterial anodes because of low bacterial loading capacity (6, 11) and/or rela-

tively poor extracellular electron-transfer efficiency (12, 13).

Considerable efforts have been devoted to improving the MFC anodic electrodes by increasing the bacteria loading capacity or enhancing the electrode conductivity (14). For example, three-dimensional electrodes with mesoporous structures could provide higher specific surface area and larger space for more bacteria loading (15, 16). Carbon nanomaterials, such as graphene (17), carbon nanotubes (18–20), and their composites with noncarbon materials (21), have been explored for reducing the charge-transfer resistance. Additionally, metal nanoparticles have been explored to improve the cell-electrode charge transfer and the current output (12, 13), whereas the exact location and the fundamental role of such nanoparticles remain elusive, and the potential of such approach to the improved MFC power output is yet to be demonstrated. Despite these strategies, the output power density of the MFCs to date has hit a plateau (8) and rarely exceeds 0.3 mW/cm^2 , which is

¹Department of Chemistry and Biochemistry, University of California, Los Angeles, Los Angeles, CA 90095, USA.

²Department of Materials Science and Engineering, University of California, Los Angeles, Los Angeles, CA 90095, USA. ³Department of Bioengineering, University of California, Los Angeles, Los Angeles, CA 90095, USA. ⁴California NanoSystems Institute, University of California, Los Angeles, Los Angeles, CA 90095, USA. ⁵Department of Earth Sciences, University of Southern California, Los Angeles, CA 90089, USA.

*Corresponding author. Email: xduan@chem.ucla.edu (X.D.); yhuang@seas.ucla.edu (Y.H.)

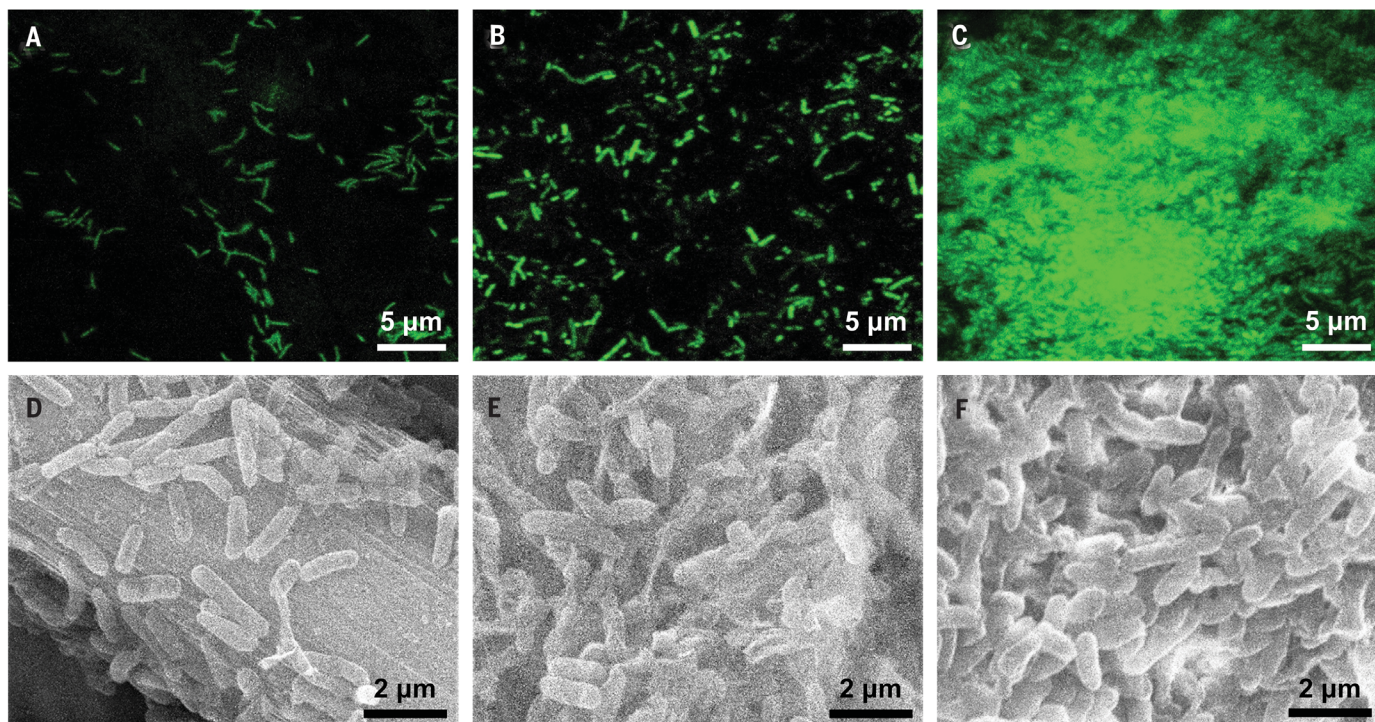


Fig. 1. Characterization of *Shewanella* biofilms. (A to C) Confocal laser scanning microscopy (CLSM) images of the *Shewanella* biofilms on (A) carbon paper, (B) rGO, and (C) rGO/Ag. (D to F) Scanning electron microscopy (SEM) images of the biofilms on the (D) carbon paper, (E) rGO, and (F) rGO/Ag.

likely due to limited efficiencies in transmembrane and extracellular electron-transfer processes (22).

Within the bacteria in MFCs, the electrons produced by catabolic processes in the bacterial cytoplasm are transferred to the electrode surface through a series of direct or indirect electron-transfer processes (fig. S1) (23–25). Overall, the transmembrane and extracellular electron-transfer processes generally involve sluggish electron hopping through redox centers in atypical conductors or through multiple redox cycles, which could severely limit the charge-transfer efficiency. Therefore, to break through the power limit of the current MFCs, it is essential to design anodic electrodes that can fundamentally address these charge-transfer limitations to efficiently extract the metabolic electrons to the external electrodes (26, 27).

Here, we report a rational strategy to boost the transmembrane and extracellular electron-transfer processes in *Shewanella* MFCs constructed with reduced graphene oxide–silver nanoparticle (rGO/Ag) scaffolds. Our systematic studies show that the rGO/Ag can release positively charged silver ions, which facilitate *Shewanella* attachment to rGO/Ag scaffolds to form dense biofilms and produce

the *Shewanella*-Ag hybrids with greatly enhanced electron-transfer efficiency to improve the bacteria turnover frequency (TOF) and boost the overall MFC performance.

Shewanella biofilm formation

To fabricate a functional MFC, the bacteria must form dense biofilms on the anode surface to ensure efficient charge transfer from the individual bacteria to the external electrode (2), which is the origin of the MFC current and power output (28). To evaluate the effectiveness of our approach, we have used three different anodic electrode materials—carbon paper, carbon paper with rGO, and carbon paper with rGO/Ag (fig. S2)—to test the compactness and thickness of the biofilms, in which the carbon paper, the most widely and commercially available MFC anodes, and rGO are used for control experiments.

Although silver is often perceived to exhibit antibacterial properties for bacteria (29, 30), such as *Escherichia coli* (fig. S3), it does not appreciably affect the viability of *Shewanella*. In particular, our biocompatibility evaluation by a confocal laser scanning microscope (CLSM) alive-dead staining assay reveals distinct green fluorescence, which originates from the SYTO

9 dye in the living bacteria, indicating that the rGO/Ag electrode is biocompatible. The number of living cells on the rGO/Ag is larger than that on the carbon paper and the carbon paper rGO composite (Fig. 1, A to C). Ag thus does not undermine the *Shewanella* bacterial viability (viability of 93% for rGO/Ag versus 95% for carbon paper and 92% for rGO; see fig. S4 for more details).

Scanning electron microscopy (SEM) images can further reveal biofilm structures with greatly variable bacterial density (Fig. 1, D to F). Compact biofilms consisting of densely packed, bar-like bacteria (~0.5 μm by ~2 μm) are found on the rGO/Ag electrodes (Fig. 1F), whereas the biofilms formed on rGO or carbon fibers are much less dense. These SEM studies are largely consistent with the confocal fluorescence studies and demonstrate that the presence of the Ag is beneficial to denser biofilm formation.

Shewanella MFC tests and performance

Before constructing full MFCs, the output current density of the anode materials was first evaluated with a three-electrode system in an electrochemical half-cell (31). Notably, the maximum current density output from the rGO/Ag

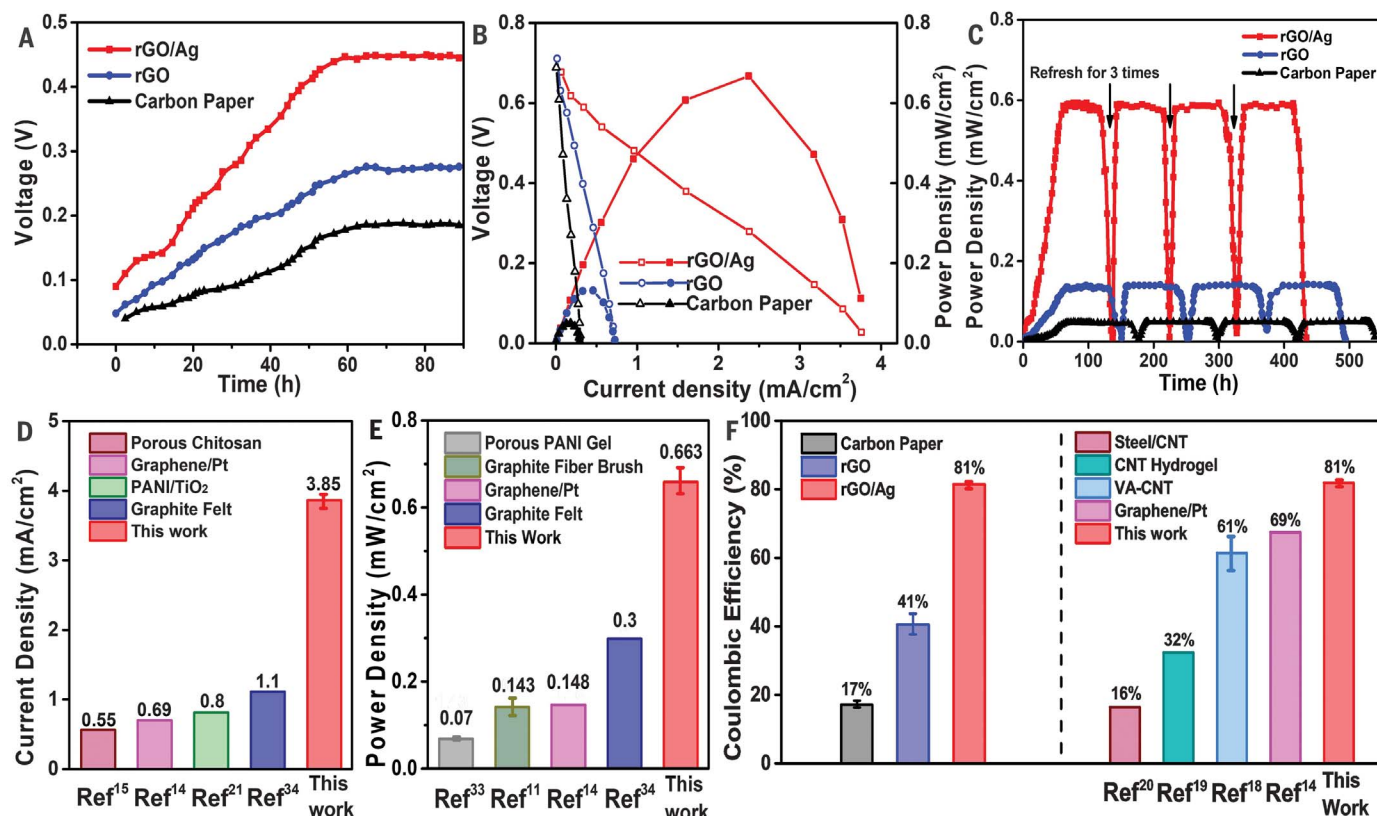


Fig. 2. Performance comparison of *Shewanella* MFCs with different anodes. (A) Voltage output of double-chamber MFCs with three different anodic materials. **(B)** *I*-*V* curves (left axis, open symbols) and power polarization (right axis, filled symbols) curves of the MFCs with three different anode materials. **(C)** MFC power density versus time curves for long-term stability and repeated cycling tests. **(D)** Comparison of the current densities with state-of-the-art MFCs. PANI, polyaniline. **(E)** Comparison of the MFC power density. **(F)** Coulombic efficiency (QE) of three different electrodes and their comparison with the state-of-art MFCs made on different electrode materials. CNT, carbon nanotube; VA, vertically aligned.

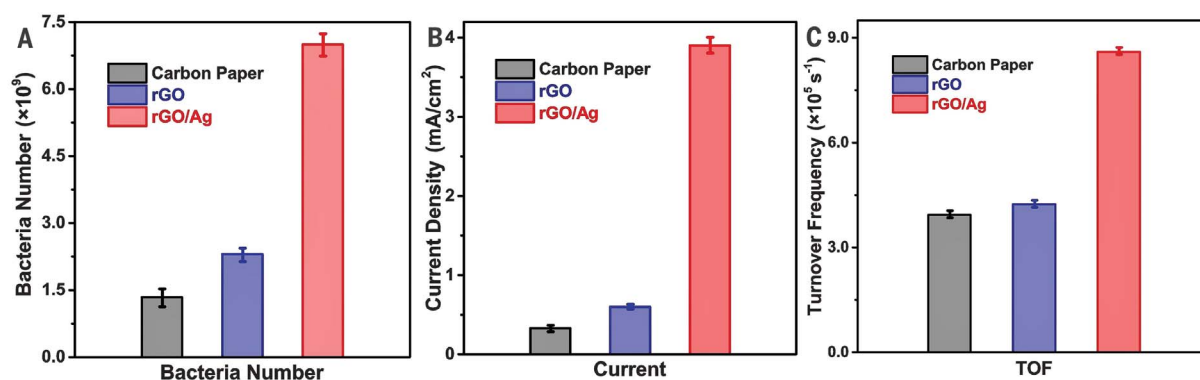


Fig. 3. Turnover frequencies (TOFs) of *Shewanella* MFCs with different anodes. (A) Comparison of bacterium number on three different electrodes. (B) Comparison of the maximum current density from three different electrodes. (C) Comparison of the calculated TOFs for the biofilms on the carbon paper, rGO, and rGO/Ag electrodes.

electrode can reach up to $0.92 \text{ mA}/\text{cm}^2$, which is considerably higher than that from either carbon paper ($0.06 \text{ mA}/\text{cm}^2$) or rGO ($0.12 \text{ mA}/\text{cm}^2$) electrodes (fig. S5).

To evaluate the power output, we have constructed the full-cell MFC device in a double-chamber container (fig. S6). The output voltage from the MFC increases continuously with incubation time and reaches a nearly constant value in ~ 2 days (Fig. 2A), indicating successful establishment of a functional MFC (14, 32). When the MFC voltage output is steady, different load resistors are connected to the anode and the cathode to obtain current versus voltage (I - V) curves and power polarization curves (Fig. 2B). The I - V curves show a similar open-circuit voltage around 0.7 V for all three electrodes, which is consistent with the maximum voltage output from similar MFCs. Notably, the rGO/Ag electrode shows a maximum current output of $3.85 \pm 0.05 \text{ mA}/\text{cm}^2$, which is much higher than that from carbon paper ($0.34 \text{ mA}/\text{cm}^2$) or rGO ($0.62 \text{ mA}/\text{cm}^2$) electrodes (Fig. 2D). The maximum power density from the rGO/Ag electrode reaches up to $0.66 \pm 0.03 \text{ mW}/\text{cm}^2$, which is also much larger than that for carbon paper anodes ($0.05 \text{ mW}/\text{cm}^2$) or rGO anodes ($0.13 \text{ mW}/\text{cm}^2$). Such enhancements of current and power output by Ag nanoparticles are reproducible across multiple measurements (fig. S7). The output current and power observed in the *Shewanella* biofilm on rGO/Ag electrode are also higher than those reported previously with other electrode materials such as polyaniline (PANI) gel (33), graphite felt (34), and others (Fig. 2, D and E, and table S2).

We have also evaluated the output performance of the MFCs over long-term operation. Voltage output from the MFC drops sharply after ~ 80 hours of stable operation, which can be attributed to the exhaustion of the nutrient in the anode medium. We conducted a cyclic test by periodically refreshing the anodic medium with nutrient when the voltage output drops below 0.05 V (Fig. 2C).

After adding the new medium with lactate as the nutrient, the output power density is rapidly restored to its original value, which confirms that the voltage drop is due to nutrient exhaustion. Similar behavior is observed for all three types of electrodes. On the basis of the amount of nutrient added and total charge output for each cycle, we can also derive the coulombic efficiency of the MFCs. The MFC with rGO/Ag anode shows a coulombic efficiency of $\sim 81\%$, much higher than those with carbon paper ($\sim 17\%$) and rGO ($\sim 41\%$) anodes and those reported previously (Fig. 2E and table S3), which indicates more-efficient use of the nutrients for power generation.

Enhanced TOFs and charge-extraction efficiency

The increased current density from the rGO/Ag anode could be attributed to a larger number of bacteria in the anode biofilm or to more-efficient charge transport and less charge loss owing to the improved charge-transfer process. To decouple these two potential factors, we quantified and compared the number of bacteria in each type of anode by combining the hemocytometer and total nitrogen analysis kit (fig. S8). With the estimated bacteria number for each electrode (Fig. 3A) and the maximum current output (Fig. 3B), we calculated the TOF for the bacteria on each electrode (Fig. 3C). Overall, the carbon paper and rGO electrodes show a comparable TOF ($\sim 3.9 \times 10^5/\text{s}$ for carbon paper and $\sim 4.2 \times 10^5/\text{s}$ for rGO), whereas the rGO/Ag electrode shows a TOF about twofold higher ($\sim 8.6 \times 10^5/\text{s}$), which indicates much higher electron extraction and transport efficiency in the rGO/Ag electrode.

The transmembrane structure of *Shewanella*-Ag hybrids

To elucidate the origin of the enhanced charge-extraction efficiency and the boosted TOFs in rGO/Ag electrode, we have conducted scanning transmission electron microscopy (STEM) and energy-dispersive x-ray spectroscopy (EDX) elemental mapping studies of the bacteria on

the rGO/Ag anode after a complete MFC cycle. The STEM and EDX mapping studies reveal enrichment of Ag around the *Shewanella* (Fig. 4A). To evaluate the spatial distribution of Ag within an individual bacterium, we have conducted STEM image and EDX elemental mapping studies on ultrathin sections of *Shewanella*-Ag hybrids. Notably, we found abundant Ag nanoparticles near, inside, and across the membrane area of the *Shewanella* cells (Fig. 4B). The formation of Ag nanoparticles near the membrane area is not surprising considering the heavy metal tolerance of *Shewanella* and the well-known metal reduction capability of these types of bacteria (4, 10). In this case, a likely scenario is that the rGO/Ag electrode slowly releases the silver ions, which diffuse toward *Shewanella* and are reduced in situ by the electrons generated by *Shewanella* metabolism to form Ag nanoparticles on and in the cytoplasmic membrane.

High-resolution STEM images and the corresponding EDX mapping images show that some Ag nanoparticles traverse the entire periplasmic space between the inner and outer membranes and break through the outer membrane (Fig. 4C). In membrane-associated cytochromes involved in transmembrane and extracellular electron-transfer processes, electrons are transferred through multistep hopping processes between $\text{Fe}^{3+}/\text{Fe}^{2+}$ redox centers (35). Because the metal electronic conductivity is far higher than the redox center-mediated charge-transfer process in cytochromes (membrane or nanowires) (36, 37), the transmembrane and outer-membrane Ag nanoparticles can potentially act as metallic shortcuts to bypass the sluggish electron-transfer process mediated by the redox centers, making direct contacts with external electrodes for more-efficient charge extraction.

Electrochemical impedance analysis

We conducted electrochemical impedance spectroscopy (EIS) studies to understand the roles of the Ag nanoparticles in the charge-transfer

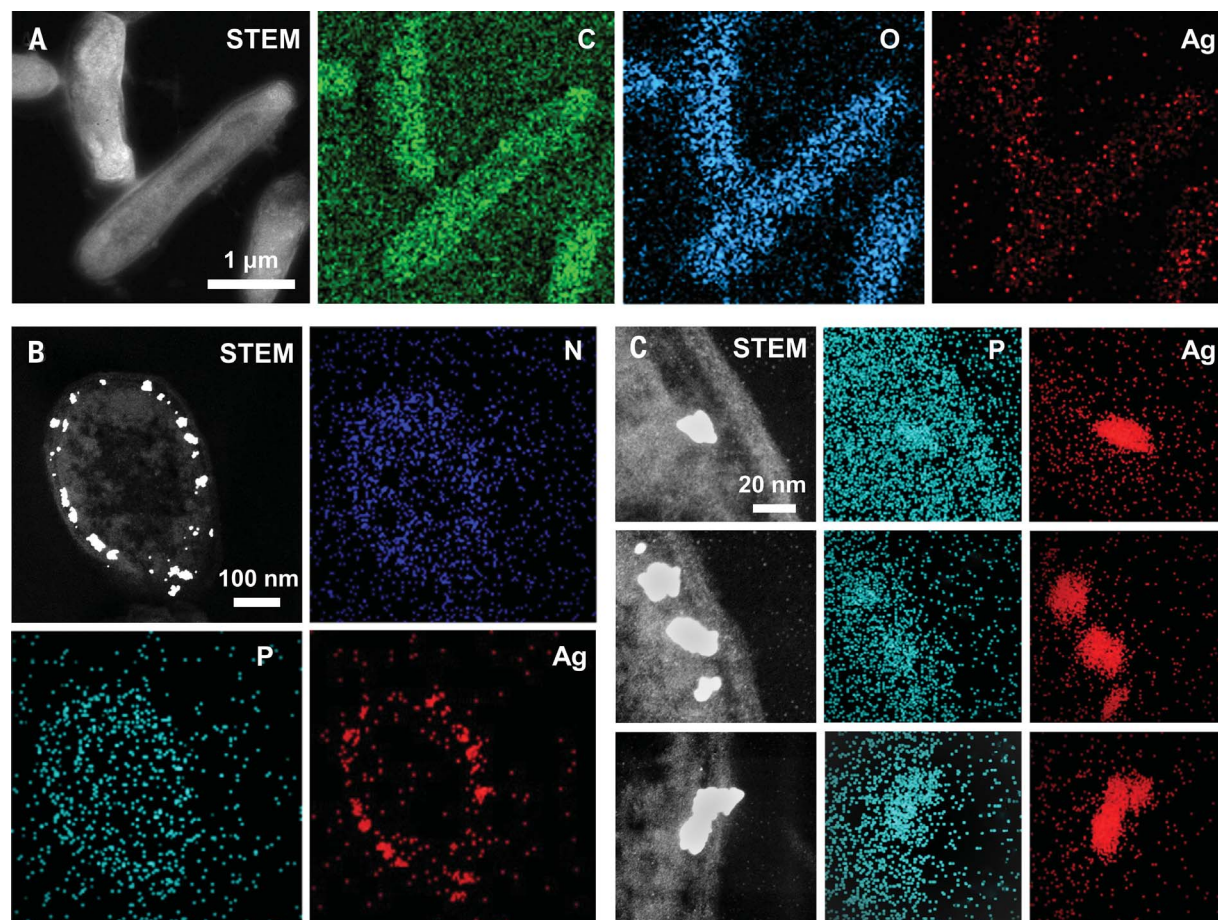


Fig. 4. Characterization of transmembrane structure of single bacterium. (A) STEM image and EDX elemental (carbon, oxygen, and silver) mapping of the bacteria on the rGO/Ag electrode. (B) STEM image and EDX mapping of the ultrathin sections of the bacteria on the rGO/Ag electrode. (C) STEM image and EDX elemental mapping of the transmembrane silver nanoparticles inside and traversing the cell membranes.

process. From the outset, both the electrochemical surface area and EIS (fig. S9) studies show rather similar values for rGO and rGO/Ag electrodes without biofilm, suggesting that the Ag nanoparticles in rGO electrode architecture do not play a notable role in the charge-transfer process and cannot explain the much higher TOFs observed in the biofilms on rGO/Ag electrode. We have further conducted EIS studies on all three types of MFCs, consisting of bacterial biofilm anodes made on carbon paper, rGO, and rGO/Ag. The Nyquist plots (Fig. 5) show two semicircles that can be attributed to the charge-transfer processes in cathode and anode (see fig. S10 for the equivalent circuit). The first semicircle for all three types of device gives a comparable charge-transfer resistance of ~ 7 ohms, which represents the contribution from the cathode reaction and is largely independent of the anode reaction, as also identified by the same semicircles shown in the MFC blank tests (fig. S11). The second semicircle originates from the *Shewanella* biofilm and gives distinct charge-transfer resistance values (R_{biofilm}) of 482, 102,

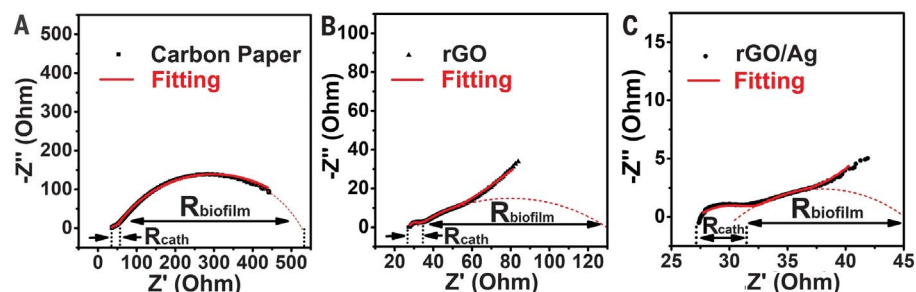


Fig. 5. EIS tests. (A to C) EIS of the biofilms on three different electrodes: (A) carbon paper, (B) rGO, and (C) rGO/Ag along with the fitting curves. The R_{cath} is the charge-transfer resistance of ferricyanide cathode reactions. The R_{biofilm} is the charge-transfer resistance from the anode bacteria biofilm. $-Z''$, xxx; Z' , xxxx.

and 16 ohms for the anodes with carbon paper, rGO, and rGO/Ag, respectively. It is apparent that the charge-transfer resistance of the biofilm on the rGO/Ag electrode is much lower than that of the other two electrodes, which can be attributed to increased numbers of bacteria and, especially, the improved transmembrane and extracellular electron-transfer efficiency due to the Ag nanoparticles. In par-

ticular, the improved TOFs in rGO/Ag electrode are largely attributed to the increased electron-transfer efficiency.

Under anaerobic conditions with the lactate as the sole nutrient, electrons transferred extracellularly mostly originate from lactate oxidation by lactate dehydrogenase (LDH) (38). It is therefore instructive to compare the TOFs achieved in our *Shewanella* biofilm

with those achieved in individual enzyme or in inorganic catalysts for similar reactions. Considering that the approximate number of copies of LDH in a bacterium is ~1000 (39, 40), the TOFs estimated for single LDH are 394/s for normal *Shewanella* and 860/s for *Shewanella*-Ag hybrids, which compare favorably to those reported for isolated LDH (TOF ~ 170 to 300/s) (41, 42). The higher TOFs achieved in the *Shewanella*-Ag hybrids suggest a critical role for the transmembrane Ag nanoparticles in boosting the charge-extraction and transfer efficiency. We note that the TOFs achieved in LDH in the *Shewanella* biofilms are several orders of magnitude higher than those achieved in lactate dehydrogenation inorganic catalysts (~0.03/s) (43), which highlights the merits of exoelectrogenic bacteria in catalyzing lactate oxidation. Together with our rGO/Ag anodic electrode, high-density *Shewanella* biofilms enable MFCs with improved power output and coulombic efficiency. *Shewanella*-metal hybrids thus provide an effective pathway to break the electron-transfer limitations of natural bacteria and push the limit of the MFCs.

REFERENCES AND NOTES

- K. Rabaey, W. Verstraete, *Trends Biotechnol.* **23**, 291–298 (2005).
- L. Lu *et al.*, *Nat. Sustain.* **1**, 750–758 (2018).
- B. E. Logan, K. Rabaey, *Science* **337**, 686–690 (2012).
- B. E. Logan, *Nat. Rev. Microbiol.* **7**, 375–381 (2009).
- B. E. Logan, J. M. Regan, *Trends Microbiol.* **14**, 512–518 (2006).
- B. E. Logan *et al.*, *Environ. Sci. Technol.* **40**, 5181–5192 (2006).
- D. Simonsson, *Chem. Soc. Rev.* **26**, 181–189 (1997).
- D. R. Lovley, *Nat. Rev. Microbiol.* **4**, 497–508 (2006).
- H. H. Hau, J. A. Gralnick, *Annu. Rev. Microbiol.* **61**, 237–258 (2007).
- B. E. Logan, R. Rossi, A. Ragab, P. E. Saikaly, *Nat. Rev. Microbiol.* **17**, 307–319 (2019).
- H. Liu, R. Ramnarayanan, B. E. Logan, *Environ. Sci. Technol.* **38**, 2281–2285 (2004).
- X. Jiang *et al.*, *Nano Lett.* **14**, 6737–6742 (2014).
- X. Wu *et al.*, *Angew. Chem. Int. Ed.* **50**, 427–430 (2011).
- S. Zhao *et al.*, *Sci. Adv.* **1**, e1500372 (2015).
- Z. He, J. Liu, Y. Qiao, C. M. Li, T. T. Y. Tan, *Nano Lett.* **12**, 4738–4741 (2012).
- Y. Yuan, S. Zhou, Y. Liu, J. Tang, *Environ. Sci. Technol.* **47**, 14525–14532 (2013).
- C. Zhao *et al.*, *J. Mater. Chem. A Mater. Energy Sustain.* **1**, 12587–12594 (2013).
- H. Ren *et al.*, *J. Power Sources* **273**, 823–830 (2015).
- X. W. Liu *et al.*, *ACS Appl. Mater. Interfaces* **6**, 8158–8164 (2014).
- Y. Zhang, J. Sun, Y. Hu, S. Li, Q. Xu, *J. Power Sources* **239**, 169–174 (2013).
- Y. Qiao *et al.*, *ACS Nano* **2**, 113–119 (2008).
- R. Wang *et al.*, *Adv. Mater.* **30**, e1800618 (2018).
- T. Fu *et al.*, *Nat. Commun.* **11**, 1861 (2020).
- M. Ding *et al.*, *ACS Nano* **10**, 9919–9926 (2016).
- M. Y. El-Naggar *et al.*, *Proc. Natl. Acad. Sci. U.S.A.* **107**, 18127–18131 (2010).
- S. Cestellos-Blanco, H. Zhang, J. M. Kim, Y. Shen, P. Yang, *Nat. Catal.* **3**, 245–255 (2020).
- N. Kornienko, J. Z. Zhang, K. K. Sakimoto, P. Yang, E. Reisner, *Nat. Nanotechnol.* **13**, 890–899 (2018).
- Y. Wang *et al.*, *ACS Nano* **10**, 6331–6337 (2016).
- Z. M. Xiu, Q. B. Zhang, H. L. Puppala, V. L. Colvin, P. J. J. Alvarez, *Nano Lett.* **12**, 4271–4275 (2012).
- Q. L. Feng *et al.*, *J. Biomed. Mater. Res.* **52**, 662–668 (2000).
- U. Schröder, J. Niessen, F. Scholz, *Angew. Chem. Int. Ed.* **42**, 2880–2883 (2003).
- X. Xie *et al.*, *Nano Lett.* **11**, 291–296 (2011).
- R.-B. Song *et al.*, *J. Mater. Chem. A Mater. Energy Sustain.* **4**, 14555–14559 (2016).
- B. R. Ringeisen *et al.*, *Environ. Sci. Technol.* **40**, 2629–2634 (2006).
- L. Shi *et al.*, *Nat. Rev. Microbiol.* **14**, 651–662 (2016).
- M. Breuer, K. M. Rosso, J. Blumberger, *Proc. Natl. Acad. Sci. U.S.A.* **111**, 611–616 (2014).
- M. Y. El-Naggar, Y. A. Gorby, W. Xia, K. H. Nealson, *Biophys. J.* **95**, L10–L12 (2008).
- E. D. Brutinel, J. A. Gralnick, *Appl. Environ. Microbiol.* **78**, 8474–8476 (2012).
- J. A. H. Wodke *et al.*, *Mol. Syst. Biol.* **9**, 653 (2013).
- G. S. Rule, E. A. Pratt, C. C. Q. Chin, F. Wold, C. Ho, *J. Bacteriol.* **161**, 1059–1068 (1985).
- G. E. Pinchuk *et al.*, *Proc. Natl. Acad. Sci. U.S.A.* **106**, 2874–2879 (2009).
- K. M. LeVan, E. Goldberg, *Biochem. J.* **273**, 587–592 (1991).
- W. Zhang *et al.*, *ACS Catal.* **8**, 2365–2374 (2018).

ACKNOWLEDGMENTS

Funding: We acknowledge the support from Office of Naval Research (grant no. N00010141712608). We acknowledge the Electron Imaging Center at UCLA for STEM technical support and the Advanced Light Microscopy/Spectroscopy at UCLA for CLSM technical support. We are grateful to J. A. Gralnick in the University of Minnesota for providing *Shewanella* mutants. **Author contributions:** Y.H. and X.D. designed the research. B.C. developed the rGO/Ag approach, fabricated the microbial fuel cell devices, performed the experiments, and conducted data analysis. B.C. and Z.Z. collected the STEM and elemental mapping images. B.C., L.P., and D.Z. designed and discussed the EIS measurements and result analysis. B.C. and H.-Y.S. cultured the *Shewanella* bacteria with the assistance of C.L., B.C., and M.D. and developed the half-cell tests system. F.S., J.H., and X.G. characterized the materials. G.C.L.W., C.L., K.N., and P.S.W. contributed to discussions. X.D. and Y.H. supervised the research. B.C., Y.H., and X.D. cowrote the paper with input from all authors. **Competing interests:** An invention disclosure on MFC fabrication has been submitted to UCLA patent office [UC. Case No. 2022-005-1 (102352-0994)]. The authors declare no other competing interests. **Data and materials availability:** All data are available in the manuscript or the supplementary materials.

SUPPLEMENTARY MATERIALS

<https://science.org/doi/10.1126/science.abf3427>

Materials and Methods

Figs. S1 to S11

Tables S1 to S4

MDAR Reproducibility Checklist

20 October 2020; resubmitted 20 April 2021

Accepted 28 July 2021

10.1126/science.abf3427



Silver nanoparticles boost charge-extraction efficiency in *Shewanella* microbial fuel cells

Bocheng Cao, Zipeng Zhao, Lele Peng, Hui-Ying Shiu, Mengning Ding, Frank Song, Xun Guan, Calvin K. Lee, Jin Huang, Dan Zhu, Xiaoyang Fu, Gerard C. L. Wong, Chong Liu, Kenneth Neelson, Paul S. Weiss, Xiangfeng Duan, and Yu Huang

Science, **373** (6561), .

DOI: 10.1126/science.abf3427

Silver in the linings

The bacterium *Shewanella oneidensis* is well known to use extracellular electron sinks, metal oxides and ions in nature or electrodes when cultured in a fuel cell, to power the catabolism of organic material. However, the power density of microbial fuel cells has been limited by various factors that are mostly related to connecting the microbes to the anode. Cao *et al.* found that a reduced graphene oxide–silver nanoparticle anode circumvents some of these issues, providing a substantial increase in current and power density (see the Perspective by Gaffney and Minteer). Electron microscopy revealed silver nanoparticles embedded or attached to the outer cell membrane, possibly facilitating electron transfer from internal electron carriers to the anode. —MAF

View the article online

<https://www.science.org/doi/10.1126/science.abf3427>

Permissions

<https://www.science.org/help/reprints-and-permissions>

Use of this article is subject to the [Terms of service](#)

Science (ISSN) is published by the American Association for the Advancement of Science. 1200 New York Avenue NW, Washington, DC 20005. The title *Science* is a registered trademark of AAAS.

Copyright © 2021 The Authors, some rights reserved; exclusive licensee American Association for the Advancement of Science. No claim to original U.S. Government Works